Electrodeposition in Capillaries: Bottom-up Micro- and Nanopatterning of Functional Materials on Conductive Substrates

Antony George, A. Wouter Maijenburg, Michiel G. Maas, Dave H. A. Blank, and Johan E. ten Elshof*

Inorganic Materials Science, MESA+ Institute for Nanotechnology, University of Twente, P. O. Box 217, 7500 AE Enschede, The Netherlands

S *Supporting Information*

ABSTRACT: A cost-effective and versatile methodology for bottom-up patterned growth of inorganic and metallic materials on the micro- and nanoscale is presented. Pulsed electrodeposition was employed to deposit arbitrary patterns of Ni, ZnO, and FeO(OH) of high quality, with lateral feature sizes down to 200−290 nm. The pattern was defined by an oxygen plasma-treated patterned PDMS mold in conformal contact with a conducting substrate and immersed in an electrolyte solution, so that the solid phases were deposited from the solution in the channels of the patterned mold. It is important that the distance between the entrance of the channels, and the location where deposition is needed, is kept limited. The as-formed patterns were characterized by high resolution scanning electron microscope, energy-dispersive X-ray analysis, atomic force microscopy, and X-ray diffraction.

KEYWORDS: soft-lithography, oxides, electrodeposition, micropatterning
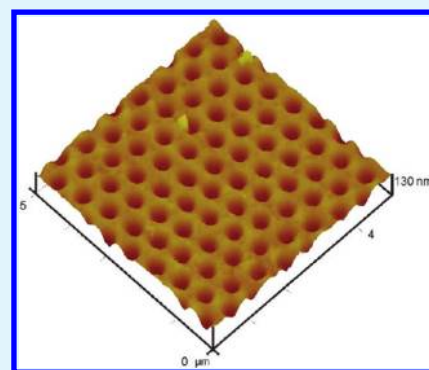
INTRODUCTION

Fast and cost-effective realization of high resolution complex patterns of functional materials is crucial in future manufacturing technologies. Patterning techniques such as photolithography,[1,2] electron beam lithography,[3] ion beam lithography,[4] nanoimprint lithography,[5] and scanning probe lithographic methods[6,7] are used in industry and research for patterning functional materials. However, all these techniques require either cleanroom processing conditions or the use of resist materials often with complex processing steps of wet/dry etching. Some of these methods are slow due to their serial nature. Well-known alternatives developed by the Whitesides research group are the soft lithographic methods that use micro/nanopatterned polydimethylsiloxane (PDMS) molds and stamps in conformal contact with a substrate as a template for site-selective patterning with functional materials.[8] Interesting features of soft lithography are its technical simplicity, low capital investment cost, and effectiveness in producing large-scale functional patterns of arbitrary materials.[8,9] The soft lithographic techniques can be divided into printing and molding-based methods and include microcontact printing,[10] micromolding in capillaries (MIMIC),[11] micromolding,[12,13] microtransfer molding,[14] edge lithography,[15] solvent assisted micro-molding,[16] nanotransfer printing,[17] and gas phase pattern deposition.[18] These methods can be used for the fabrication of different functional patterns including self-assembling molecules, metals, metal oxides, nanoparticles, bio-molecules, and polymeric materials.

Electrodeposition is a simple, scalable, and cost effective tool for fabricating inorganic functional thin films of metals,[19,20] metal alloys,[21,22] metal oxides,[23] and conducting polymers[24] on conductive substrates. Electrodeposition using templates such as patterned photoresist,[1,2] polycarbonate membranes,[25] anodic alumina membranes,[26] colloidal crystals,[27] and self-assembled monolayers[19,28] attracted a lot of research and industrial interest due to its ability to fabricate 2D and 3D patterns of inorganic functional materials,[1,2,19] nanowires,[25,26] and nanotubes.[25] As is shown below, a combination of soft lithography and electrodeposition can be used as a tool for large area patterning of various functional materials on micrometer and nanometer scale. In comparison with other combinations of deposition and lithographic techniques to generate functional material patterns, the combination of electrodeposition and soft lithography is technically versatile and cost effective as it can be carried out under normal ambient conditions, without the use of complex patterning, etching, and deposition steps.

In the present paper, we demonstrate the possibility of a single step, bottom-up, inexpensive, and easy process for 2D nano- and micropatterning of functional material on conductive substrates by electrodeposition using patterned PDMS molds as templates. A schematic diagram of the patterning process is shown in Figure 1. A PDMS mold with micrometer or nanometer scale channels is gently pressed against a conductive substrate. A connected channel structure is formed between the substrate and the PDMS mold. The substrate—mold assembly is immersed in an electrolyte solution and used as working electrode to deposit functional materials like nickel, platinum, zinc oxide (ZnO), and
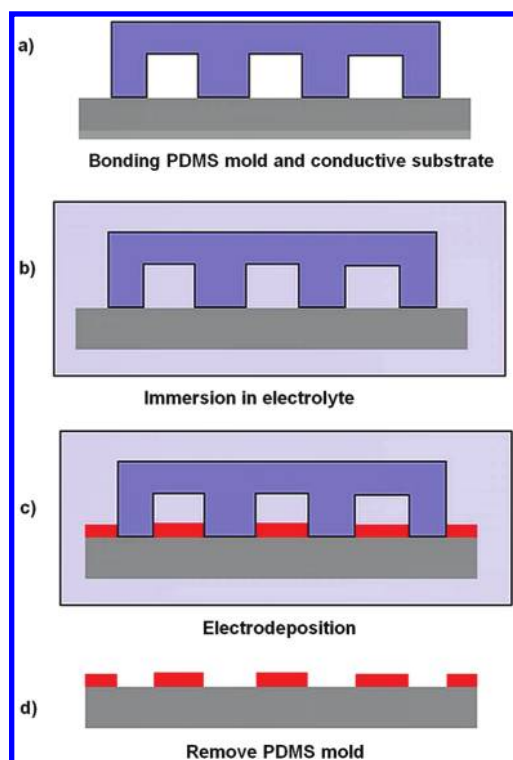
Figure 1. Procedure of electrodeposition in capillaries. (a) Bonding the substrate and the patterned PDMS mold. (b) Immersion in the electrolyte solution for several minutes to assure proper filling of the channels. (c) Electrodeposition inside the capillaries to form the material patterns. (d) Peeling off the mold from the substrate and washing in de-ionized water.

iron oxohydroxide $(FeO(OH))$. We demonstrated patterns with a size range of 180 nm to a few micrometers.

■ EXPERIMENTAL SECTION

Fabrication of PDMS Templates. PDMS and curing agent (Sylgard 184) were purchased from Dow Corning Corporation, mixed in a mass ratio of 10:1, and poured over a patterned silicon wafer that was coated with a 1H,1H,2H,2H-perfluorooctylsilane monolayer as an anti-adhesion layer. The micrometer scale masters were patterned by standard photolithography, and the patterns were transferred to the Si substrate by etching (Lionix BV, Netherlands). The nanometer scale masters were purchased from LightSmyth Technologies, Inc., USA. The PDMS was cured at a temperature of 70°C for 24 h. After curing, the PDMS substrates were removed from the master and cut into pieces of desired size.

Substrate Preparation. P-type silicon wafers with a sputtered gold film of thickness ~75 nm, deposited with a Perking-Elmer sputtering machine, were used as substrates. A titanium film of ~10 nm thickness was used as an adhesion promotion layer between the silicon wafer and the gold thin film.

Electrodeposition in Capillaries. The patterned PDMS molds were placed in an oxygen plasma cleaner (Harrick plasma, operating at 240 W) for 5 min prior to bonding with the substrate. The surface oxidation process increased the hydrophilicity of the mold to promote filling of the channels by the aqueous electrolyte. After plasma treatment, the patterned side of the molds was gently pressed against the substrate and the mold—substrate assembly was immersed in the electrolyte for 5 min to assure proper filling of the entire channels. The PDMS mold—substrate assembly was placed vertically inside the electrodeposition cell.

Good conformal contact is required to be able to obtain well-defined features.

Electrodeposition was carried out using a three-electrode potentiostat (Autolab PGSTAT 128N from Metrohm Autolab, Netherlands). The substrate—PDMS assemblies were used as working electrodes. A small Pt mesh was used as counter electrode. The reference electrode was Ag/AgCl in 3M KCl (Metrohm Autolab). Nickel patterns were formed from an electrolyte containing 0.23 M nickel sulphate hexahydrate $(NiSO_4 \cdot 6H_2O$, Sigma-Aldrch, purity 99%,) and 0.15 M boric acid $(H_3BO_3$, Aldrich, purity 99.99%). Deposition occurred at -1.00 V versus reference. Zinc oxide patterns were formed at 70°C at -1.00 V from an electrolyte containing 0.10 M zinc nitrate hexahydrate $(Zn(NO_3)_2 \cdot 6H_2O$, Sigma-Aldrich, purity 98%,). Iron oxohydroxide patterns were formed at -1.00 V from an electrolyte containing 0.02 M iron nitrate nonahydrate $(Fe(NO_3)_3 \cdot 9H_2O$, Sigma-Aldrich), 0.430 M nitric acid $(HNO_3$, 65% solution, Arcos Organics), and 0.425 M sodium hydroxide (NaOH, pellets, Sigma-Aldrich). Further details can be found elsewhere.[25]

In the deposition of Ni and ZnO, we applied pulsed potential electrodeposition. In most experiments, after every 5 s of deposition (T_{on}), the deposition was stopped for the next 120 s (T_{off}), by returning to open circuit potential (OCP), and these steps were repeated for any desired number of times. We also used other values for T_{on} and T_{off}, depending on the dimensions of the PDMS template and the electrolyte used for electrodeposition. In the case of $FeO(OH)$, we used continuous potentiostatic electrodeposition for 5 min. Prior to electrodeposition the mold—substrate assembly was immersed in the electrolyte solution for 30 min to ensure complete filling of the channels. After deposition, the PDMS molds were removed from the substrate and the substrates were washed with de-ionized water, dried using a nitrogen stream, and stored for further analysis.

Characterization. Patterned substrates were characterized using tapping mode atomic force microscopy (AFM; Veeco Dimension Icon) to determine the surface morphology. Grown metal and oxide patterns were imaged using high resolution scanning electron microscopy (HR-SEM, Zeiss 1550) and tapping mode AFM. X-ray diffraction (XRD, Philips diffractometer PW 3020, Software XPert Data Collector 2.0e, Panalytical B.V., Almelo, The Netherlands) was used for phase determination of the patterns. Energy dispersive X-ray spectroscopy (EDX) mapping was performed using a NORAN EDS spectrometer.

■ RESULTS AND DISCUSSION

Figure 2a shows the SEM image of a Ni pattern formed on an Au-coated silicon substrate by electrodeposition. Figure 2b,c,d shows a tapping mode AFM image, a tapping mode 3D AFM image, and an AFM height profile, respectively. The PDMS molds of area $\sim5 \times 5$ mm^2 that were used in this experiment have an ordered array of pillars with a diameter of 1.5 μm, a height of 6 μm, and a repeat distance of 3 μm. Deposition was carried out in 5 intervals of 2 min each. After every 2 min of deposition, the deposition was stopped for the next 2 min without applying any potential. This time period allowed fresh Ni ions to diffuse into the channels to replace the deposited nickel ions. The patterns grew to a thickness of approximately 100 nm after 10 min of deposition.

The 3D AFM topography image and the AFM height profile show the sharp ring-like formation protruding at the periphery of every circular pit. Every ring has a width of approximately 200 nm at its base and a height of 80—100 nm. The ring formation is probably the result of an increased metal ion concentration at the surface of the PDMS molds. The oxygen plasma treatment of the PDMS mold prior to bonding with the gold substrate forms an amorphous SiO_x-rich surface layer on PDMS that
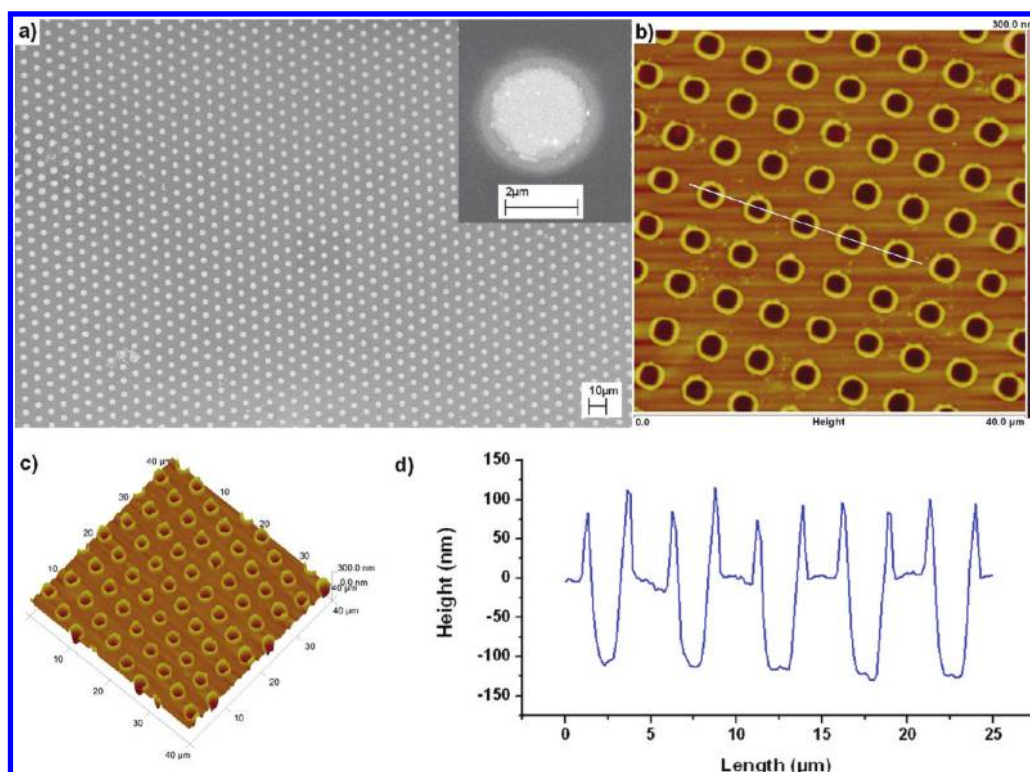
Figure 2. Images of Ni patterns formed on gold-coated silicon substrate after 10 min of electrodeposition. (a) HR-SEM image; (b) AFM height image; (c) 3-D surface image; (d) AFM height profile. The deposition was carried out in 5 intervals of 2 min, each separated by 2 min intervals in which no potential was applied.
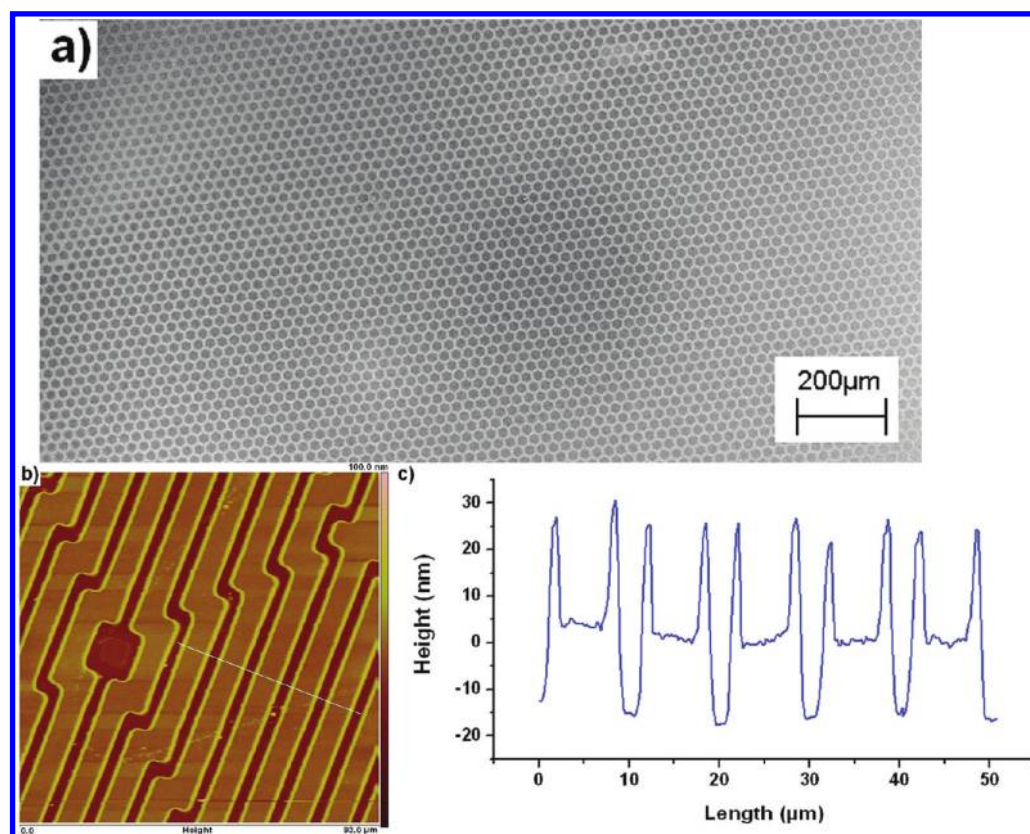

Figure 3. Ni patterns on gold-coated silicon substrate after 2 min of continuous electrodeposition. (a) SEM image of honeycomb pattern. (b, c) Tapping mode AFM image and AFM height profile of complex line patterns.
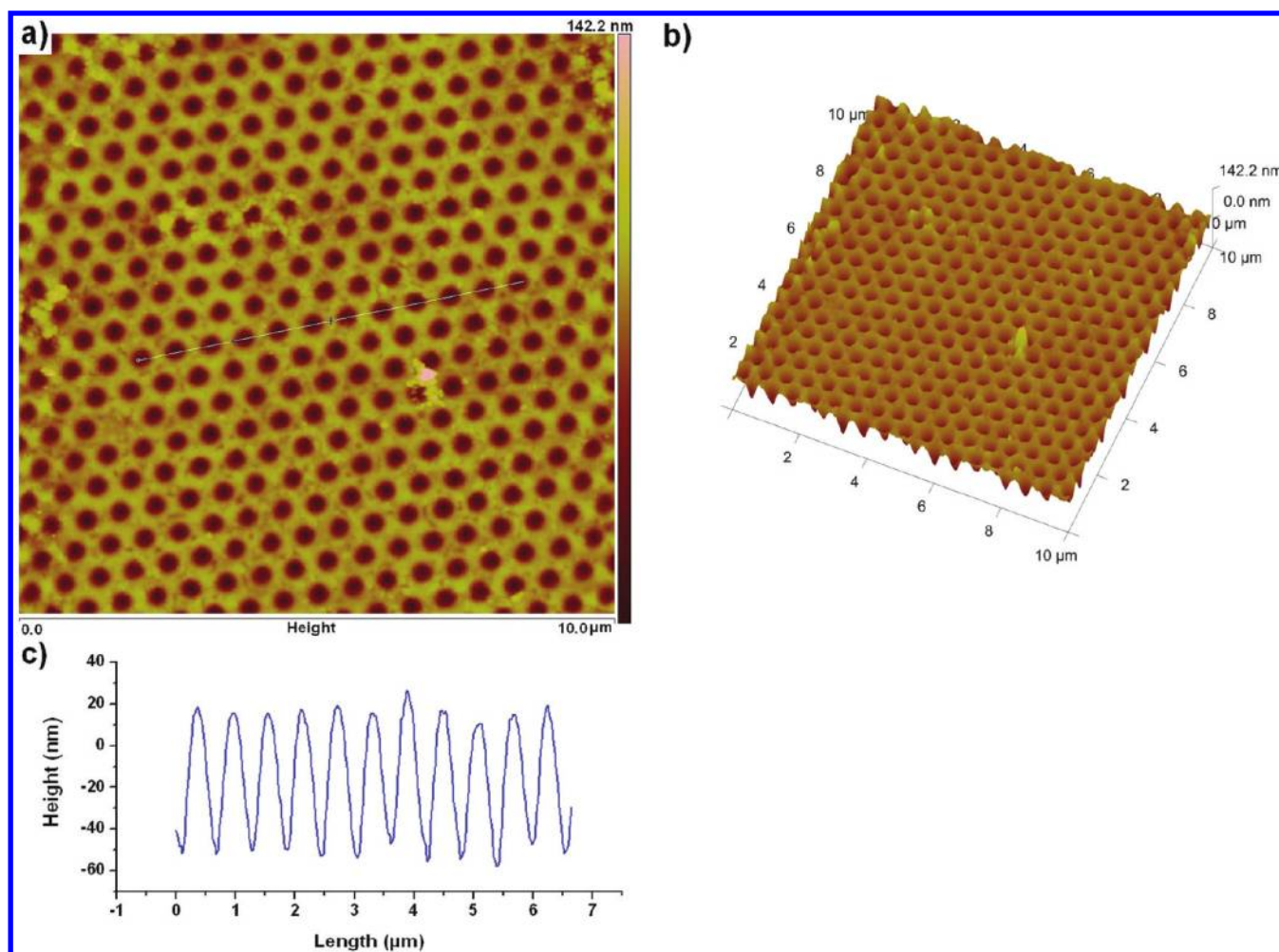
Figure 4. Nanoscale antidot Ni patterns on Au-coated silicon substrate after 150 s of deposition at −1.00 V. Deposition was carried out in 30 cycles of 5 s, with an interval of 2 min between cycles in which no current was applied. (a) AFM height image; (b) 3D surface image; (c) AFM height profile.
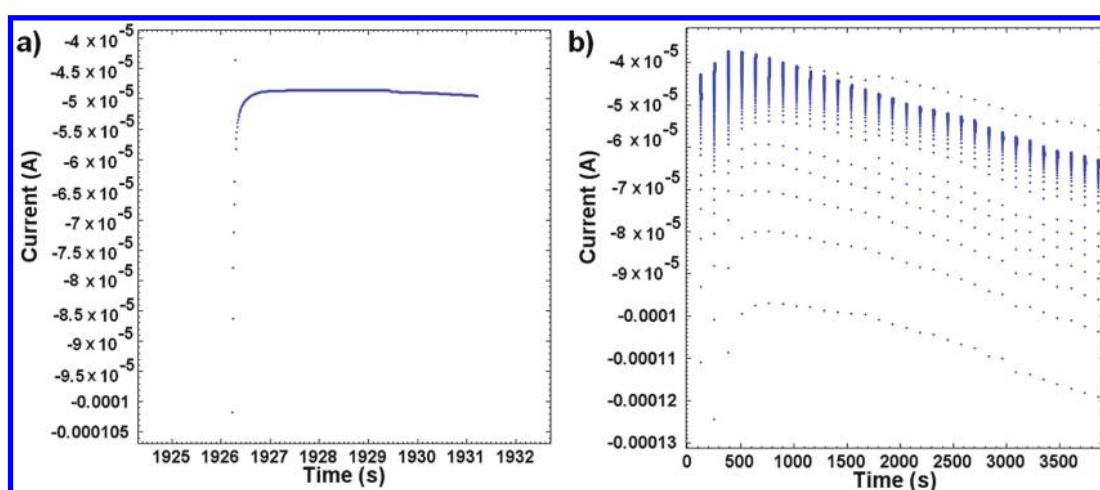
Figure 5. (a) Chronoamperogram of pulsed Ni deposition inside nanoscale PDMS molds. Potentiostatic deposition lasted 5 s at −1.00 V. Waiting time between pulses was 2 min. (b) Chronoamperogram of the complete deposition process.

becomes negatively charged in aqueous solutions above the isoelectric point (IEP) of silica at pH = 2 to 3. Since we worked at pH 4, the negative ζ-potential of the surface oxide leads to

an increased concentration of ions with a positive charge, in particular doubly charged ions, in the diffuse double layer near the surface. As a result, the local deposition rate of Ni is higher

3669

dx.doi.org/10.1021/am200852w |*ACS Appl. Mater. Interfaces* 2011, 3, 3666–3672
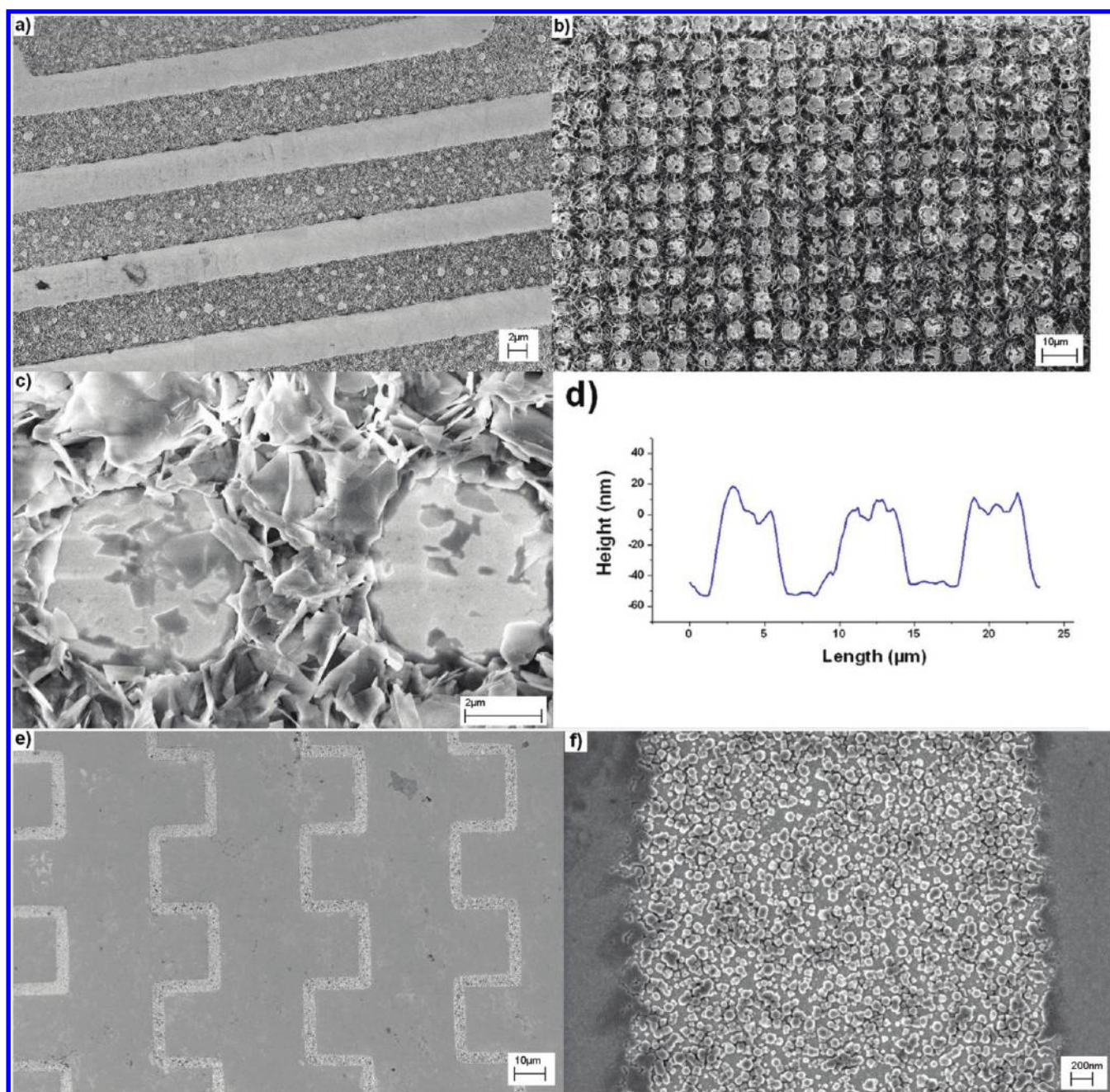
Figure 6. ZnO patterns on Au-coated silicon substrate. (a, b) ZnO patterns formed after 5 cycles of cathodic deposition. $T_{on} = 1$ min, $T_{off} = 2$ min. (c) Magnified view of ZnO pattern morphology of panel b. d) AFM height profile of ZnO pattern of panel b. (e) ZnO nuclei on Au coated Si substrate after 10 deposition pulses. $T_{on} = 1$ s, $T_{off} = 1$ min. (f) Magnified view of ZnO pattern of Figure 5e.

than further away from the PDMS walls and ultimately forms ring-like structures.

The pulsed electrodeposition technique was employed due to the fact that the ion concentration inside the channels of the mold is depleted during the deposition process. In order to maintain a uniform concentration of ions throughout the channels, deposition was stopped for a period of time to allow fresh reactants to diffuse into the channels and to reach a uniform electrolyte concentration throughout the channels, before the next deposition pulse was initiated. The T_{on} and T_{off} times have to be carefully tuned in order to achieve uniform film thickness over the channels. The average diffusion distance L of ions over a given interval of time t is given by

$$L^2 = nDt \tag{1}$$

where D is the self-diffusion coefficient of the ion, and $n = 6$ in the case of unconstrained molecular movement in three dimensions. In aqueous solutions, the self-diffusion coefficients of most ions are similar and have values in the range of 0.6×10^{-9} to 2×10^{-9} m²/s at room temperature. In the experiments, we employed PDMS templates with a total patterned area of 5×5 mm², and well interconnected channel structures were employed. The maximum distance between the edge to the center of the

template is approximately 2.5 mm. Considering that diffusional supply of reactant occurred from external openings at all sides of the PDMS mold, but is constrained inside the channels due to the presence of walls on a length scale of micrometers, the diffusion process is quasi-two-dimensional in this case, so that n is approximately 4. Then, the time scale for replenishment t is of the order of ~100 seconds. The diffusion lengths can be reduced by engineering the PDMS mold, e.g., by constructing a few larger access channels between smaller channels, and/or by making access channels from the top side of the PDMS molds.

We also tested continuous potentiostatic electrodeposition of Ni. However, it did not result in high quality patterns when the PDMS molds did not have very well-connected channel structures. Probably, in this case, the diffusional supply of Ni^{2+} into the channels of the PDMS mold was smaller than the rate of consumption of nickel ions inside the channels. However, when a PDMS mold with well connected channel structure and large channel dimensions were employed, continuous potentiostatic reduction of Ni^{2+} also yielded high quality patterns, as illustrated in Figure 3 for a honeycomb pattern of Ni, fabricated by continuous deposition for 2 min at −1 V. The PDMS mold, with a patterned area of ~5 × 5 mm^2, had channels with a width of ~3.2 μm and a height of ~6 μm. The grown patterns have an approximate thickness of ~15 nm as measured by AFM. It was not possible to grow thicker layers by continuous deposition for longer periods of time, probably due to diffusional limitations. Longer deposition resulted in thicker films near the channel openings and thinner films in the central channels. This means that a concentration gradient of nickel ions is present in the channels, leading to a situation in which most metal ions were deposited on the substrate before reaching the middle of the channels.

We also used PDMS molds with smaller nanometer-scale features as templates. Figure 4 shows a tapping mode AFM image, an AFM height profile, and an AFM 3D topography image of a hexagonal array of Ni antidots on Au. The PDMS mold with an area of ~5 × 5 mm^2 contained a hexagonal array of circular pillars with a diameter of 290 nm and a spacing of 200 nm between the pillars. The height of the pillars was 250 nm. The pattern was fabricated by pulsed electrodeposition, using 30 cycles with T_{on} = 5 s and T_{off} = 120 s. The height profile shows that the resulting antidot pattern has a thickness of 65 nm. Figure 5a,b shows the chronoamperogram recorded during the deposition process. Figure 5a shows an example of a single 5 s deposition pulse. EDX analyses are provided in the Supporting Information file, showing that the areas where the PDMS mold was in conformal contact with the substrate and was isolated from deposition.

Figure 6a−c shows HR-SEM images of ZnO patterns formed on a gold-coated silicon substrate by pulsed electrodeposition. Each deposition pulse was 1 min, and the interval between deposition cycles was 2 min. The pattern in Figure 6a was grown in 4 pulses to a thickness of ~20 nm. The PDMS mold used has lines of width of 4.2 μm, spacing of 5.8 μm, and height of 6 μm. The patterns in Figure 6b,c were grown in 10 pulses to a thickness of ~55 nm, as illustrated in the AFM height profile of ZnO shown in Figure 6d. The PDMS mold used has square pillars of width of 4.25 μm, spacing of 3.25 μm, and height of 6 μm. The ZnO patterns formed has a flake-like porous surface morphology. Figure 6e,f shows ZnO nuclei formed as a result of applying very short deposition pulses during the deposition process. The PDMS mold used here has complex line features of width of 25 μm, spacing of 4 μm, and height of 6 μm. Each deposition pulse was for 1 s, followed by a waiting time of 1 min.
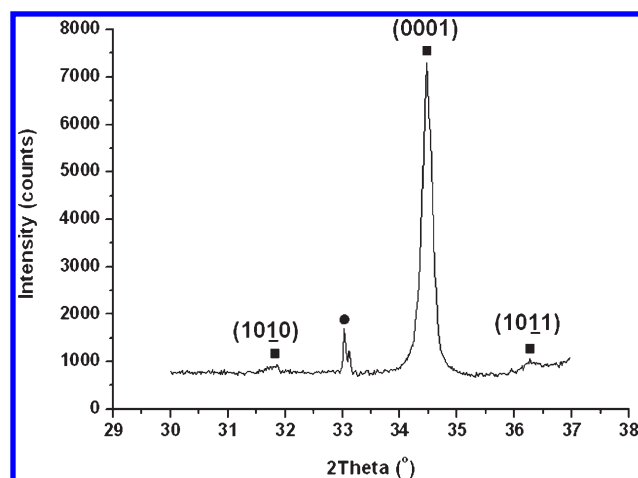

Figure 7. XRD pattern of ZnO grown on Au substrate. The peak at 2θ 34.4° corresponds to the (0002) reflection of the ZnO wurtzite structure. The squares represent ZnO pattern peaks, and the circles represent substrate peaks. The split peak at 2θ 33° is from the silicon substrate. The splitting of the silicon peak is due to the presence of K_α and K_β radiation.

The total number of deposition pulses was 10. Due to the short duration of the entire deposition process, only isolated hexagonal ZnO nuclei had formed and no further growth occurred. ZnO deposition involves the reduction of nitrate and water to hydroxyl ions, followed by precipitation of zinc hydroxide, which is directly transformed into ZnO above 60°C via:[25]

$$NO_3^- + H_2O + 2e^- \rightarrow NO_2^- + 2OH^- \tag{2}$$

$$Zn^{2+} + 2OH^- \rightarrow ZnO + H_2O \tag{3}$$

The X-ray diffractogram of the patterned wurtzite film is shown in Figure 7. The strong (0002) peak is indicative of preferential (0001) growth of the ZnO phase, which is common under these growth conditions.

Figure 8 shows a SEM image of amorphous iron oxohydroxide FeO(OH) patterns formed on a Au coated silicon substrate after 5 min of continuous deposition. First, an iron hydroxide gel formed inside the channels by precipitation of Fe^{3+} with OH^- that formed via reaction 4 at −1.00 V. The substrate−mold assembly was then dried on a hot stage at 60°C for 1 h. During drying, the iron oxohydroxide phase formed from the gel following.[25]

$$Fe^{3+} + 3OH^- \rightarrow Fe(OH)_3(aq) \rightarrow FeO(OH)(s) + H_2O \tag{4}$$
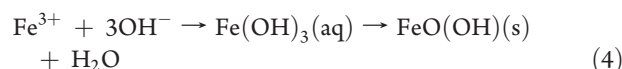
The process described here generated negative replicas of the patterns on the PDMS mold. Patterns with complex shapes such as sharp angles and curves can be prepared by this method. The process gives precise control of size and shape of the generated patterns, since the lateral dimensions are defined by the dimensions of the PDMS template used and the height is defined by the electrodeposition time. The process is a cost effective, bottom-up patterning process in which metal, metal oxide, and/or multilayered materials can be deposited. Electrodeposition is an old process which has proven its capacity to deposit a wide range of technologically important functional materials, such as metals (e.g., Ni, Au, Ag, Cu, Al), metal alloys (e.g., FePt), semiconducting
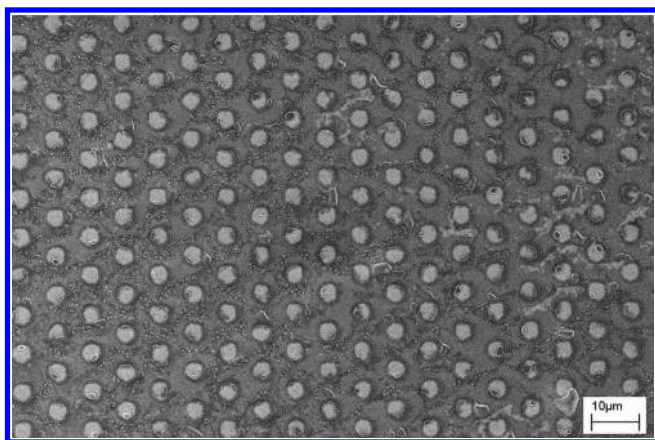
Figure 8. SEM image of FeO(OH) pattern on gold-coated silicon substrate after 5 min of continuous deposition at room temperature and 1 h of drying at 60° C.

oxides (e.g., ZnO, Fe_2O_3, TiO_2), and conducting polymers.[24] Due to low deposition temperature conditions, the process is suitable for any conductive substrate, including flexible plastic substrates with conductive coatings. We used conventional PDMS molds for the deposition experiments, but other materials could be used as well, provided that they make good conformal contact with the substrate. More research needed to design the molds with more access holes for the electrolyte from the sides as well as the top so that the process could be faster and even higher resolutions can be achieved.

CONCLUSIONS

Electrodeposition in capillaries is a promising tool for patterning nano- and microscale structures on conducting substrates, especially for bottom-up growth of metallic patterns which cannot be achievable easily by other soft lithographic patterning methods. We have patterned a wide range of functional materials including ZnO, Ni, and FeO(OH) by the technique. A wide range of materials can be patterned in micro- and nanometer scale by this technique. Further research is recommended with PDMS molds with engineered channels with more access channels for electrolyte for fast deposition over large areas of substrate.

ASSOCIATED CONTENT

ⓢ Supporting Information. EDX analysis of Ni patterns. This material is available free of charge via the Internet at http://pubs.acs.org.

AUTHOR INFORMATION

Corresponding Author
*E-mail: j.e.tenelshof@utwente.nl. Phone: +31 53 489 2695. Fax: +31 53 489 2990.

ACKNOWLEDGMENT

REFERENCES

(1) Xiang, C.; Kung, S.-C.; Taggart, D. K.; Yang, F.; Thompson, M. A.; Güell, A. G.; Yang, Y.; Penner, R. M. *ACS Nano* **2008**, *2*, 1939–1949.

(2) Menke, E. J.; Thompson, M. A.; Xiang, C.; Yang, L. C.; Penner, R. M. *Nat. Mater.* **2006**, *5*, 914–919.

(3) Balaur, E.; Djenizian, T.; Boukherroub, R.; Chazalviel, J. N.; Ozanam, F.; Schmuki, P. *Electrochem. Commun.* **2004**, *6*, 153–157.

(4) Rastei, M. V.; Meckenstock, R.; Bucher, J. P.; Devaux, E.; Ebbesen, T. *Appl. Phys. Lett.* **2004**, *85*, 2050–2052.

(5) Ko, S. H.; Park, I.; Pan, H.; Grigoropoulos, C. P.; Pisano, A. P.; Luscombe, C. K.; Frechet, J. M. J. *Nano Lett.* **2007**, *7*, 1869–1877.

(6) Ginger, D. S.; Zhang, H.; Mirkin, C. A. *Angew. Chem., Int. Ed.* **2004**, *43*, 30–45.

(7) Xu, S.; Liu, G.-y. *Langmuir* **1997**, *13*, 127–129.

(8) Xia, Y. N.; Whitesides, G. M. *Angew. Chem., Int. Ed.* **1998**, *37*, 551–575.

(9) ten Elshof, J. E.; Khan, S. U.; Göbel, O. F. *J. Eur. Ceram. Soc.* **2010**, *30*, 1555–1577.

(10) Kumar, A.; Whitesides, G. M. *Appl. Phys. Lett.* **1993**, *63*, 2002–2004.

(11) Kim, E.; Xia, Y.; Whitesides, G. M. *J. Am. Chem. Soc.* **1996**, *118*, 5722–5731.

(12) Göbel, O. F.; Blank, D. H. A.; ten Elshof, J. E. *ACS Appl. Mater. Interfaces* **2010**, *2*, 536–543.

(13) Khan, S. U.; Gobel, O. F.; Blank, D. H. A.; ten Elshof, J. E. *ACS Appl. Mater. Interfaces* **2009**, *1*, 2250–2255.

(14) Göbel, O. F.; Nedelcu, M.; Steiner, U. *Adv. Funct. Mater.* **2007**, *17*, 1131–1136.

(15) Sharpe, R. B. A.; Titulaer, B. J. F.; Peeters, E.; Burdinski, D.; Huskens, J.; Zandvliet, H. J. W.; Reinhoudt, D. N.; Poelsema, B. *Nano Lett.* **2006**, *6*, 1235–1239.

(16) Shi, G.; Lu, N.; Gao, L.; Xu, H.; Yang, B.; Li, Y.; Wu, Y.; Chi, L. *Langmuir* **2009**, *25*, 9639–9643.

(17) Lee, B. H.; Cho, Y. H.; Lee, H.; Lee, K. D.; Kim, S. H.; Sung, M. M. *Adv. Mater.* **2007**, *19*, 1714–1718.

(18) George, A.; Blank, D. H. A.; ten Elshof, J. E. *Langmuir* **2009**, *25*, 13298–13301.

(19) Pesika, N. S.; Radisic, A.; Stebe, K. J.; Searson, P. C. *Nano Lett.* **2006**, *6*, 1023–1026.

(20) Zach, M. P.; Ng, K. H.; Penner, R. M. *Science* **2000**, *290*, 2120–2123.

(21) Kleiman-Shwarsctein, A.; Hu, Y.-S.; Forman, A. J.; Stucky, G. D.; McFarland, E. W. *J. Phys. Chem. C* **2008**, *112*, 15900–15907.

(22) Liu, R.; Vertegel, A. A.; Bohannan, E. W.; Sorenson, T. A.; Switzer, J. A. *Chem. Mater.* **2001**, *13*, 508–512.

(23) Natter, H.; Schmelzer, M.; Hempelmann, R. *J. Mater. Res.* **1998**, *13*, 1186–1197.

(24) Zhou, F.; Chen, M.; Liu, W.; Liu, J.; Liu, Z.; Mu, Z. *Adv. Mater.* **2003**, *15*, 1367–1370.

(25) Maas, M. G.; Rodijk, E. J. B.; Maijenburg, A. W.; Blank, D. H. A.; ten Elshof, J. E. *J. Mater. Res.,* **2011** (Available on CJO 16 May 2011); doi:10.1557/jmr.2011.93.

(26) Routkevitch, D.; Bigioni, T.; Moskovits, M.; Xu, J. M. *J. Phys. Chem.* **1996**, *100*, 14037–14047.

(27) Yan, H.; Yang, Y.; Fu, Z.; Yang, B.; Xia, L.; Fu, S.; Li, F. *Electrochem. Commun.* **2005**, *7*, 1117–1121.

(28) Azzaroni, O.; Schilardi, P. L.; Salvarezza, R. C. *Appl. Phys. Lett.* **2002**, *80*, 1061–1063.